Characteristics of picosecond coherent anti-Stokes Raman spectroscopy with mode-locked dye lasers in comparison with stimulated Raman gain

M. De Mazière,* M. Baggen, M. van Exter,† and A. Lagendijk

Natuurkundig Laboratorium, University of Amsterdam, Valckenierstraat 65, 1018 XE Amsterdam, The Netherlands

Received January 1, 1989; accepted November 1, 1989

Time-resolved coherent anti-Stokes Raman scattering (CARS) has been performed with a double synchronously pumped mode-locked dye-laser system that is the same as had been used earlier for stimulated Raman gain (SRG) experiments; the CARS signal is also spectrally resolved. We present an extensive experimental and theoretical study of the CARS technique and compare the results with the characteristics of SRG. Experimental tests have been performed on the 656- and 991-cm^{-1} modes in liquid CS_2 and C_6H_6, respectively. In particular, the influence of the pulse chirps on the time resolutions in CARS and SRG has been examined. SRG profits from oppositely chirped dye-layer pulses. In these circumstances, the observed time resolution in SRG is typically a factor of 3 better than in CARS. Also, when measured under off-resonance conditions, CARS decay curves exhibit a narrow and pronounced coherence spike that is symmetrical near zero delay: its appearance is discussed in detail. In addition, we establish the conditions for which the phenomena of critical frequency mistuning and spectral narrowing in time-delayed CARS are observable.

1. INTRODUCTION

Picosecond time-resolved coherent anti-Stokes Raman scattering (CARS) is a well-known technique for probing the dephasing characteristics of condensed matter directly in the time domain.[1] An alternative technique is stimulated Raman gain (SRG): it has been explored by us extensively in the past.[2,3]

We have performed both kinds of experiment with the same double synchronously pumped mode-locked dye-laser system. For CARS experiments, some other groups[4–11] use a dye-laser system similar to ours, sometimes with more-intense dye laser pulses, pumped by a mode-locked and Q-switched Nd:YAG laser at a lower repetition rate (500 Hz).[11] But CARS measurements are usually performed[1,12,13] with a fixed-frequency powerful laser pulse, at a repetition rate of a few hertz, in conjunction with the Stokes-shifted counterpart generated by it. With the last-named system, the parameters of the pump and Stokes pulses are automatically interrelated. Therefore our experimental setup differs from the common one mainly in its operation at higher-repetition-rate, low average laser powers and in the fact that both pulses can be adjusted individually (see also Section 2 below). We present a detailed comparison between the characteristics and merits of both techniques, studied in an identical experimental situation.

The picosecond CARS signal is spectrally resolved, providing additional information about the evolution in time and frequency of the different constituents of the signal. This feature was recognized previously,[14] but it is not commonly taken advantage of.

The experimental study revealed two striking characteristics:

(1) Under specific experimental conditions, a sharp and narrow coherent spike was observed in the time-resolved CARS signal, at zero delay. It appears in addition to the overshoot, called a coherence peak by Kohles *et al.*,[13] which is due only to the indistinguishability of the pump and probe beams of the same frequency, at zero delay. The occurrence of artifacts was mentioned by other authors[5,8,10] in the past, but either the artifacts were of a different appearance or they were not explained thoroughly. Therefore we investigate them in detail in this paper.

(2) The time resolutions that are typically observed with our experimental setup favor SRG; for CARS they are approximately a factor of 3 worse.

In order to understand the origin of these observations, we made an extensive experimental, analytical, and numerical study of the CARS and SRG signal characteristics. In this paper we discuss the main results concerning the CARS technique and compare them with those obtained for SRG in an earlier analogous study.[2] The sensitivity of the signal features to the pulse characteristics, in particular to the pulse chirps, is clearly demonstrated. In this respect, a linear frequency chirp in the pulses has been assumed. It turns out that the dye lasers in our setup typically have a chirp of opposite sign.

In addition to the phenomena mentioned above, we have demonstrated how the appearance of a critical frequency mistuning in SRG reported by us previously[15] can be predicted from the analytical expressions. Its appearance in CARS is analyzed in the same way. Moreover, our analysis reproduces the spectral narrowing previously reported in the short-excitation–prolonged-interrogation and prolonged-ex-

0740-3224/90/050726-13$02.00

citation–short-interrogation techniques.[16] However, comments on the conditions for its observation are in order.

This paper is organized as follows: Section 2 presents our experimental setup. Section 3 sketches the theoretical derivation of the expressions for the CARS signal intensity that are studied and discussed in the rest of the paper. They are specified to the experiments under study. The model of linearly chirped Gaussian pulses is introduced. The results of the experimental and corresponding theoretical analyses are discussed in Section 4, in which the following topics are treated: the importance of the relative signs of the laser pulse chirps (Subsection 4.A), in particular, for the time resolution in CARS and SRG dephasing measurements (Subsection 4.A.1) and for the appearance of a coherent spike in the CARS experiments (Subsection 4.A.2). We show that we operate our system with oppositely chirped pulses. The next topics are the phenomenon of critical frequency mistuning (Subsection 4.B) and the spectral behavior of the CARS signal, with particular attention to the observation of spectral narrowing (Subsection 4.C). Final conclusions are drawn in Section 5.

2. EXPERIMENTAL SETUP

The experimental setup is shown schematically in Fig. 1. An acousto-optically mode-locked Ar-ion laser synchronously pumps two (Spectra-Physics) Rh6G dye lasers in tandem. They yield ~65 mW of output power if pumped with ~350 mW of power each. Both of them are tunable in frequency with an intracavity two-plate birefringent filter. For both SRG and CARS experiments, their frequency difference ($\omega_L - \omega_S$) is adjusted with respect to the energy of the Raman mode studied, i.e., to the ν_1 symmetric stretch in liquid CS_2 at 656 cm^{-1} or to the breathing mode in liquid benzene (C_6H_6) at 992 cm^{-1}.

In time-resolved CARS experiments, half of the ω_L beam is combined with the ω_S beam to provide a pump pair; the delay τ between the two beams is adjustable and should normally be zero. The other half of the ω_L beam is split off to provide a probe beam, which can be given a variable delay, t_D, with respect to the pump pair.

All three beams run parallel to the sample; the combining cube beam splitter and mirror are mounted onto translation stages to vary the distance between them. Thus the angle between the beams, which are focused in the sample with a 75-mm focal length, can be optimized for phase matching the CARS process. It has been found that the ω_S beam cannot lie between both ω_L beams. Behind the sample, the beams are recollimated (120-mm focal-length lens). The CARS beam of interest is selected with a diaphragm and focused onto the entrance slit of a Raman spectrometer unit (Spex 1401 double monochromator coupled to an SSR photon-counting unit). Unlike in most experiments reported in the literature in which the full spectral width of the anti-Stokes signal is sampled, our spectrometer bandpass is typically set narrower, namely, at ~5 cm^{-1}.

An unwanted residual at the anti-Stokes frequency originates from the spontaneous anti-Stokes signal and from the CARS signal generated by one of the ω_L beams with the ω_S beam. Each residual is limited to at most 0.5%, through suitable optimization of the phase-matching geometry and

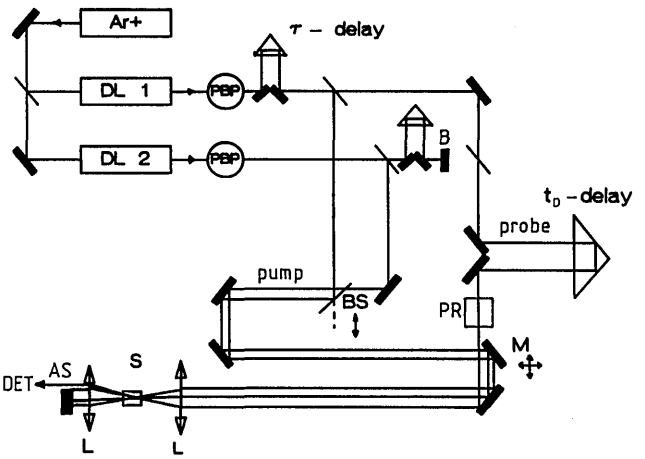

Fig. 1. Experimental setup for time-resolved CARS. Mounting of the recombining beam splitter (BS) and mirror (M) upon translation stages (⇕) permits the phase-matching conditions to be satisfied. PR, polarization rotator (additional polarizers on pump and probe that control the purity of their relative polarizations are not shown); AR^+, mode-locked Ar-ion laser; DL, dye laser; S, sample; L's, lenses; AS, anti-Stokes signal field; DET, detection unit, consisting of spectrometer plus photon counting unit; /, beam splitter; filled rectangles, mirrors. The differences for the setup for SRG[3] are the absence of modulation techniques, the insertion of a (rotatable) Pellin–Broca prism (PBP) on each dye laser beam, the parallel instead of collinear recombination of both pump beams, and blocking (B) of the DL 2 (ω_S) probe beam.

careful selection behind the sample of the signal of interest. Since these residuals represent a constant background in a CARS measurement, they are subtracted from the signal. In our CS_2 experiments, the signal-to-noise ratio thus obtained allows for a scan over ~4.5 decades; the signal strength on top is ~200 kc/sec. Moreover, in order to prevent the dye-laser fluorescence from entering the experiment, we inserted a Pellin–Broca dispersing prism of SF10 glass on each dye-laser beam immediately behind each output coupler. The spatial filtering eliminates the fluorescence. The Pellin–Broca prism is preferable to a simple 60° prism because it is a constant-deviation prism[17]: its minimum deviation angle is 90°, independently of wavelength. This experimental complication is typical of the use of dye lasers for excitation.

Two kinds of CARS experiment are performed. Either the delay between pump and probe, t_D, is scanned at a fixed spectrometer setting (detection frequency ω_D) or the spectrometer is scanned at a fixed value of t_D. Hereafter the former experiment will be called time run; the latter, spectral run. The other main parameters are the mistuning between the excitation frequency and the Raman resonance, δ_R, and the delay, τ, within the pump pair.

The 82-MHz pulse trains are monitored simultaneously in the time and frequency domains. Typical values here are ~7–9-psec autocorrelation FWHM and ~7–9-cm^{-1} spectrum FWHM. It is clear that the pulses are not transform limited. For comparison, some of the experiments were conducted with an additional étalon (900-GHz free spectral range) in one or both of the dye-laser cavities. The étalon broadens the pulse width by less than a factor of 2 while reducing the spectral width by more than a factor of 3 (typi-

cally ~10–15-psec autocorrelation FWHM and ~1.5–3-cm^{-1} spectrum FWHM). Thus the extent to which the pulses deviate from being transform limited is reduced from approximately 100–150% to approximately 20–40%.[18] The excess spectral width is attributed solely to a linear frequency chirp (see Section 3 below). The above values are only indicative: the actual values are rather sensitive to dye-laser alignment and cavity length.

Usually all interacting laser beams have parallel (vertical) polarization. A polarization rotator in the probe beam allows us to switch to an orthogonal pump–probe polarization configuration (see Fig. 1).

3. THEORETICAL CARS ANALYSIS

The emitted CARS signal was analyzed within the same theoretical framework as was done by us previously for SRG measurements.[2,3] SI units are adopted. In brief, the emitted anti-Stokes field (frequency ω_{AS}) is related to the macroscopic third-order polarization at the same frequency, $P_{AS}^{(3)}(x, t)$, through the macroscopic Maxwell equations. These are linearized in the slowly varying envelope approximation, corresponding with the fact that we are dealing with a low-power cw mode-locked laser system. Also, the small-gain limit holds. Thus

$$\frac{\partial}{\partial x}\tilde{E}_{AS}(x, t) = \frac{i\mu_0\omega_{AS}^2}{2k_{AS}}\tilde{P}_{AS}^{(3)}(x, t)\exp[i(k_P - k_{AS})x], \quad (1)$$

where t is the retarded time and μ_0 is the magnetic permeability of the vacuum. All waves are assumed to propagate as plane waves along x; $\mathbf{k}_P$ and $\mathbf{k}_{AS}$ are the wave vectors of $\mathbf{P}_{AS}$ and $\mathbf{E}_{AS}$, respectively. According to the slowly varying envelope approximation, the nonlinear polarization amplitude $P^{(3)}(x, t)$ is written as

$$P^{(3)}(x, t) = \sum_{\omega}\left\{\frac{1}{2}\tilde{P}_{\omega}^{(3)}(x, t)\exp[i(kx - \omega t)] + \text{c.c.}\right\}, \quad (2)$$

and analogously for the electric field amplitude $E(x, t)$. The sum over ω points to the discrete frequency components of relevance, for instance in E, the applied laser fields at frequencies ω_L and ω_S, and the signal field at frequency $\omega_{AS} = 2\omega_L - \omega_S$. Tildes are used for distinguishing the envelope amplitudes in the slowly varying envelope approximation from the total amplitudes; they are omitted hereafter because only the envelope amplitudes still enter the equations.

The response of the probed material to the incident fields is treated in the Born–Oppenheimer approximation for isotropic media.[19] Unlike for SRG, the Kerr effect does not contribute to the polarization at the anti-Stokes frequency. Two-photon absorption is negligible in the liquids studied. Therefore only the electronic response and the nuclear response of the excited Raman vibration are included. On the picosecond time scale, the former response is instantaneous and thus completely characterized by its strength σ; the latter is a time-dependent function, denoted by $d_R(t)$.

In analogy with Refs. 2 and 3, the complex envelope amplitude $P_{AS}^{(3)}(x, t)$ of the nonlinear polarization becomes

$$\begin{aligned}P_{AS}^{(3)}(x, t) = (1/4)\epsilon_0\exp(i\omega_L t_D)\Big\{&(3/2)\sigma E_L(t)E_L(t - t_D)E_S^*(t)\\ &+ \int_{-\infty}^{t} dt' d_R(t - t')E_L(t - t_D)E_L(t')E_S^*(t')\\ &\times\exp[i(\omega_L - \omega_S)(t - t')]\\ &+ \int_{-\infty}^{t} dt' d_R(t - t')E_L(t)E_L(t' - t_D)E_S^*(t')\\ &\times\exp[i(\omega_L - \omega_S)(t - t')]\Big\}. \quad (3)\end{aligned}$$

With respect to the time-resolved CARS signal, only those contributions that are generated by the common action of the three input laser beams have been kept. The pump beam envelopes are represented by $E_L(t)$ and $E_S(t)$; the delayed probe beam envelope, by $E_L(t - t_D)$. The corresponding wave vectors are $\mathbf{k}_L$, $\mathbf{k}_S$, and $\mathbf{k}_{L'}$, respectively, and the nonlinear polarization of Eq. (3) has wave vector $\mathbf{k}_P = \mathbf{k}_L + \mathbf{k}_{L'} - \mathbf{k}_S$. The terms containing the integrals in Eq. (3) result from interchanging the roles of the ω_L pump and probe beams; we will come back to this important point below.

The wave-vector geometry is assumed to satisfy the phase-matching requirements $\mathbf{k}_{AS} = \mathbf{k}_L + \mathbf{k}_{L'} - \mathbf{k}_S$, and the anti-Stokes signal is selected in the direction of $\mathbf{k}_{AS}$. Thus Eq. (3) lists the phase-matched contributions.

Finally, the Raman response for the mode at frequency ω_R is specified as

$$d_R(t) = id_R\exp(-t/T_2)\exp(-i\omega_R t)\Theta(t) + \text{c.c.}, \quad (4)$$

in which d_R is proportional to the differential Raman cross section, integrated over the linewidth, and $\Theta(t)$ is the unit step function. After introducing δ_R for the mistuning between the excitation and the Raman resonance:

$$\delta_R = \omega_R - (\omega_L - \omega_S), \quad (5)$$

one arrives at

$$\begin{aligned}P_{AS}^{(3)}(t) = (1/4)\epsilon_0\exp(i\omega_L t_D)\Big\{&(3/2)\sigma E_L(t)E_L(t - t_D)E_S^*(t)\\ &+ id_R E_L(t)\int_{-\infty}^{t} dt'\\ &\times\exp[-(t - t')(1/T_2 + i\delta_R)]E_L(t' - t_D)E_S^*(t')\\ &+ id_R E_L(t - t_D)\int_{-\infty}^{t} dt'\\ &\times\exp[-(t - t')(1/T_2 + i\delta_R)]E_L(t')E_S^*(t')\Big\}. \quad (6)\end{aligned}$$

The electric field envelope amplitude $E_{AS}(t)$ is simply proportional to $P_{AS}^{(3)}(t)$, because in our simplified description the integration of $E_{AS}(x, t)$ over the sample length L [see Eq. (1)] is reduced to a multiplication by the phase-mismatch factor. This factor tends to L in the limit of perfect phase matching, making the proportionality factor equal to $i\mu_0\omega_{AS}^2 L/(2k_{AS})$.

The CARS pulse is passed through the spectrometer. If

this spectrometer bandpass is centered at the detection frequency ω_D and has width Δ, the detected CARS signal $S(\delta_D, t_D)$ is essentially the squared modulus of the Fourier transform of the nonlinear polarization at frequency δ_D, denoted below as $P_{AS}^{(3)}(\delta_D)$, integrated over Δ. δ_D is defined as

$$\delta_D = \omega_D - \omega_{AS}. \tag{7}$$

As a result, $S(\delta_D, t_D)$ can be written as

$$S(\delta_D, t_D) = \frac{\mu_0 c}{8}\left(\frac{\omega_{AS}}{n_{AS}}\right)^2 L^2 \int_\Delta d\delta_D \int_{-\infty}^{+\infty} d\tau \times \langle P_{AS}^{(3)*}(0) P_{AS}^{(3)}(\tau)\rangle \exp(i\delta_D \tau), \tag{8}$$

in which n_{AS} is the linear refractive index at frequency ω_{AS} and

$$\langle P_{AS}^{(3)*}(0) P_{AS}^{(3)}(\tau)\rangle = \int_{-\infty}^{+\infty} dt P_{AS}^{(3)*}(t) P_{AS}^{(3)}(t+\tau). \tag{9}$$

Equation (8) tells that the detected CARS signal is determined by the first-order correlation function of the nonlinear polarization at the anti-Stokes frequency. In this way pulse-coherence properties enter into consideration. It is also important to note that the different contributions to $P_{AS}^{(3)}$ interfere in the signal.

In Eqs. (8) and (9) all fields are assumed to have parallel polarization; we shall comment on the orthogonal polarization configuration when discussing the corresponding results. Although not shown explicitly above, the algebraic development and corresponding numerical analysis of the basic equation [Eq. (6)] optionally include a delay τ within the pump pair and jitter between the ω_L and the ω_S fields; the jitter is averaged over a block distribution. Additional Raman lines (e.g., from isotopes or hot bands) can be accounted for by adding to Eq. (6) Raman terms that are characterized by different numerical values of the parameters d_R, T_2, and δ_R.

The pulse model adopted is that of a linearly chirped Gaussian:

$$E_L(t) = (a_L/\pi)^{1/4} \exp(-A_L t^2), \tag{10}$$

$$A_L = a_L(1 - i\beta_L)/2,\ a_L = 4 \ln 2/{t_{p,L}}^2, \tag{11}$$

with $t_{p,L}$ the intensity FWHM of the L pulse. β_L is the chirp parameter: it broadens the pulse spectral width, $\Delta\omega_L$, from $[4(\ln 2)a_L]^{1/2}$ to $[4(\ln 2)a_L(1+\beta_L^2)]^{1/2}$ FWHM. β_L positive (negative) corresponds to downchirp (upchirp). The proportionality factor normalizes the total pulse energy. Analogous relationships hold for $E_S(t)$.

The expressions thus obtained for the separate contributions to $P_{AS}^{(3)}(\delta_D)$ are

$$\Sigma(\delta_D) \propto (a_L {a_S}^{1/2}/A)^{1/2} \exp(-\gamma),$$

$$B(\delta_D) \propto (a_L {a_S}^{1/2}/A)^{1/2} \exp(-\gamma)\sqrt{1/\alpha}\, w(i\zeta/\sqrt{\alpha}),$$

$$C(\delta_D) \propto (a_L {a_S}^{1/2}/A)^{1/2} \exp(-\gamma)\sqrt{1/\alpha}\, w(i\zeta'/\sqrt{\alpha}),$$

with

$$-\gamma = \frac{1}{A}[-A_L(A_L + A_S^*)(t_D+\tau)^2 + 2A_L A t_D \tau - \tfrac{1}{4}{\delta_D}^2 + iA_L(t_D+\tau)\delta_D],$$

$$\zeta/\sqrt{\alpha} = \frac{1}{2\sqrt{\alpha}}\left\{\left(\frac{1}{T_2} + i\delta_R\right) + \frac{A_L}{A}[2A_L t_D - 2(A_L + A_S^*)\tau] - i\frac{A_L + A_S^*}{A}\delta_D\right\},$$

$$\zeta'/\sqrt{\alpha} = \frac{1}{2\sqrt{\alpha}}\left\{\left(\frac{1}{T_2} + i\delta_R\right) - \frac{A_L}{A}[2(A_L + A_S^*)t_D - 2A_L\tau] - i\frac{A_L + A_S^*}{A}\delta_D\right\},$$

and

$$w(z) = \exp(-z^2)\mathrm{erfc}(-iz),$$

$$A = 2A_L + A_S^*,$$

$$\alpha = \frac{A_L}{A}(A_L + A_S^*), \tag{12}$$

and proportionality factors that are independent of the pulse parameters. Σ is the electronic contribution, and B and C are Raman contributions; they correspond to the first, second, and third terms, respectively, in Eqs. (3) and (6). The symmetry between the B and C Raman contributions makes their analytical expressions follow from each other by interchanging τ with t_D.

So far all laser and signal fields have been assumed to have parallel polarization, according to our common experimental situation, and in Eq. (4) the anisotropic part of the Raman response function has been neglected. If the last assumption is dropped, then the response functions obeyed by both Raman contributions remain mutually identical in the parallel-polarization configuration but become mutually different for B and C in the orthogonal-polarization configuration, as stated explicitly in Ref. 20. Thus a comparison between both polarization configurations allows us to identify the distinct roles of the two Raman contributions. With the use in our numerical simulations of the correct parameters for the 656-cm^{-1} mode in liquid CS_2,[21] the purely anisotropic contribution turns out to be negligibly small. Consequently, we adopted the approximation the B Raman term contribution to the total CARS signal being equal to zero.

Now conclusions drawn from this analysis are discussed and compared with experimental data. We also discuss the distinction between CARS and SRG, making use of our previous analyses of the SRG characteristics.[2,3,15]

4. RESULTS AND DISCUSSION

To permit a comparison between experimental data and numerical simulations of CARS and/or SRG, the pulse parameters introduced in Eq. (11) must be quantized. It should be pointed out that different contributions to the CARS or SRG signal are governed by different correlation functions. For instance, in SRG[2] the electronic and Raman contributions are characterized by an identical correlation function that is, however, different from that which governs the Kerr contribution. In CARS the correlation function that governs the second Raman contribution, labeled B in Eq. (12), differs from the one that governs the electronic and C Raman contributions. Furthermore, the correlation func-

tions governing equivalent contributions in both techniques are mutually different. In consequence of this, the separate pulse parameters need to be evaluated if one requires that all contributions to the CARS or SRG signal be simulated correctly or if a comparison between both techniques is desired on the basis of an identical experimental situation. The simulations of SRG experiments presented in Ref. 15 are not adequate in this respect because they use only one substituting parameter, namely, the FWHM of the SRG electronic contribution correlation width.

The present numerical data explain the essential features of the corresponding experiments. The separate pulse-parameter values, used simultaneously in the SRG and CARS simulations, have been selected in agreement with the experimental pulse data (see Section 2). From the pulse spectral width, the chirp parameter is derived to have an absolute value of 2 (±0.5) or of less than 1 (±0.5), depending on whether the dye-laser cavity does not or does contain an étalon, respectively. Its sign cannot be determined from this measurement.

It turns out that the following characteristics of CARS and SRG are highly sensitive to the relative signs of the chirps of both dye lasers: the characteristic time resolution, the appearance of a coherent spike in CARS time runs, and some spectral characteristics of both SRG and CARS. They are discussed in Subsection 4.A in the same order. Apparently all of them hint at oppositely chirped dye lasers.

The study of time resolution also gives us a way to improve the resolution by intentionally altering the pulse parameters.

A. Influence of Chirp

1. *Comparison of Time Resolution between CARS and SRG*

As a measure of time resolution, we consider the FWHM, R_t, of the system response curve, which is defined as the time-resolved signal measured under off-resonant excitation conditions. R_t determines the lower limit of T_2 that can be resolved. The Gaussian pulse model adopted [Eqs. (10) and (11)] yields a Gaussian system response curve for both SRG and CARS experiments. In SRG experiments it is essentially a four-field correlation function, with FWHM equal to[2]

$$R_t(\mathrm{SRG}) = 4\left\{\frac{\ln 2}{(a_L + a_S)[1 + (a_L\beta_L - a_S\beta_S)^2/(a_L + a_S)^2]}\right\}^{1/2}, \quad (13)$$

whereas in CARS it is essentially a six-field correlation function, with FWHM equal to

$$R_t(\mathrm{CARS}) = 2\left\{\ln 2\,\frac{2 + a_S/a_L}{(a_L + a_S) + a_L a_S{}^2(\beta_L + \beta_S)^2/[(2a_L + a_S)^2 + (2a_L\beta_L - a_S\beta_S)^2]}\right\}^{1/2}. \quad (14)$$

Notice that the above formulas are sensitive only to the relative sign of β_L and β_S.

The above formulas [Eqs. (13) and (14)] will now be evaluated for some limit situations of the pulse parameters. First, in the limit that the pulses are unchirped Gaussians, R_t(SRG) reduces to $2t_{p,L}/[1 + t_{p,L}{}^2/t_{p,S}{}^2]^{1/2}$, or to $t_p\sqrt{2}$ for pulses of equal width t_p, whereas, similarly, R_t(CARS) reduces to $t_{p,L}\{[2 + t_{p,L}{}^2/t_{p,S}{}^2]/[1 + t_{p,L}{}^2/t_{p,S}{}^2]\}^{1/2}$ and to $t_p\sqrt{3/2}$, respectively. Hence, as long as the ratio of the L to S pulse width is smaller than $\sqrt{2}$, the time resolution in CARS is slightly better than in SRG. Second, the effects of chirp are considered. In the limit of β_L and β_S going to infinity and having equal signs, and for pulses of width t_p, the resolution of CARS experiments tends to $t_p/\sqrt{2}$, while that of SRG experiments remains $t_p\sqrt{2}$. The same limit conditions but with β_L and β_S having mutually opposite signs yield the same resolution as in the $\beta_L = \beta_S = 0$ case for CARS experiments but make the SRG resolution tend to 0 following a $1/\beta$ dependence.

The above considerations explain the time resolutions observed by us; we refer to the next subsection for experimental CARS data and to Refs. 2, 3, and 15 for SRG data. If equivalent experimental situations are compared, the time resolution in our CARS measurements is typically a factor of 3 worse than in our SRG measurements. Our setup typically uses oppositely chirped dye-laser pulses.

In addition, the basic expressions [Eqs. (13) and (14)] are used for evaluating numerically the dependence on pulse envelope width and chirp of time resolution on the one hand and signal strength on the other hand. In particular, the Raman contributions that exhibit the T_2 relaxation (i.e., in CARS experiments, the C Raman term) have been considered. Starting with transform-limited pulses, two basically different ways of changing the system's time resolution by introducing chirp are distinguishable. Either the pulses' spectral widths are kept fixed while their time envelope widths are enlarged, e.g., in a grating-compression setup, or else the pulses keep a constant envelope width in the time domain but are spectrally broadened; this happens, for instance, after transmission through a fiber because of nonlinear refractive-index effects. When we adopt pulse parameters that are typical of our experimental setup, it turns out numerically that time resolution improves only in the latter case; the corresponding behavior of the strength of the relevant Raman contributions in SRG and CARS experiments is illustrated in Fig. 2. Different combinations of chirp signs have been compared; for CARS as well as for SRG, the results are independent of a simultaneous change of both (L and S) chirp signs. The most striking difference between the SRG and CARS results is the fact that only in SRG experiments is the dependence of the Raman signal strength on time resolution independent of the chirp configuration by which this resolution is obtained. This results from the fact that the only determinant parameter is $|a_L\beta_L - a_S\beta_S|$ with respect to strength as well as to time resolution. The examples of Fig. 2 prove the usefulness of deliberately generating chirped pulses for improving the system's time resolution, especially for SRG experiments: time resolution can be improved by a factor of 2, while the Raman signal strength decreases by less than a factor of 2. The situation is less favorable in CARS experiments: at best (in the up–up or down–down

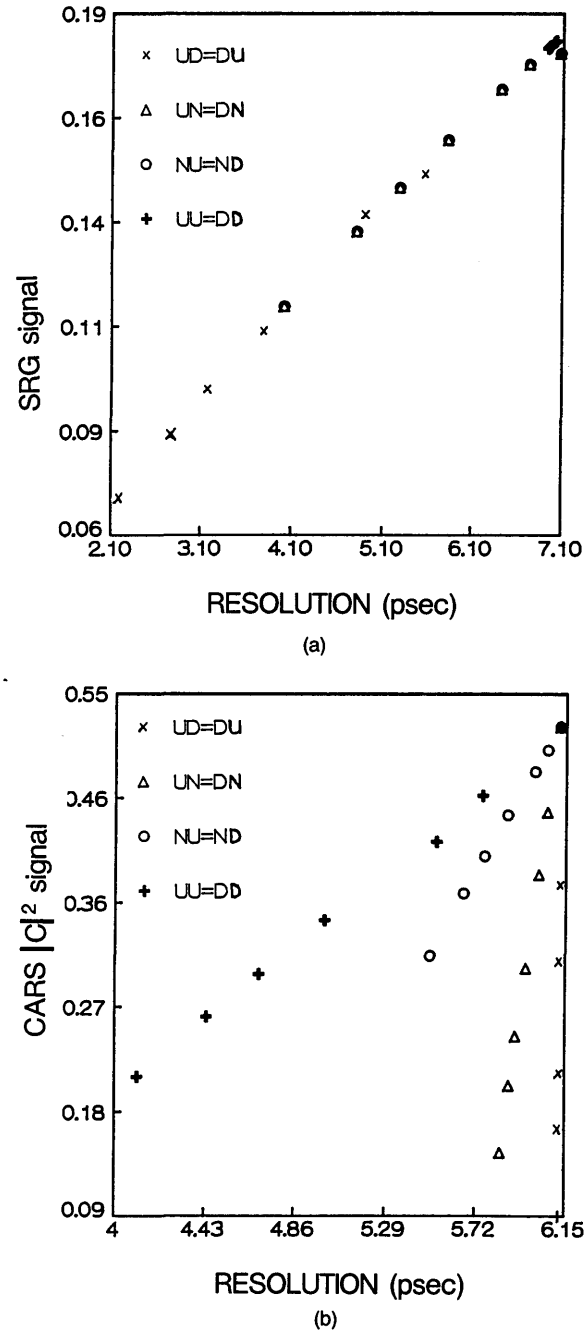

Fig. 2. Signal strength of the main Raman contributions to (a) the SRG and (b) the CARS signals versus time resolution. L and S laser pulse spectral widths have been varied, while their time envelope widths are fixed ($t_{p,L} = t_{p,S} = 5.0$ psec). The different curves correspond to different chirp configurations, as identified at the top left; here the first (second) letter specifies the L (S) laser pulse frequency chirp, with U indicating an upchirp, D a downchirp, and N no chirp.

configuration), the Raman signal strength has dropped by a factor of 2 when the time resolution has improved by only 25%.

2. Behavior of the Coherent Spike in CARS Time Runs

The results shown in Fig. 3 are typical for the experimental occurrence of the coherent spike in our time-resolved CARS measurements of the dephasing of the symmetric stretch in liquid CS_2 at room temperature. The origin of the spike should be understood so there will be no misinterpretation of the CARS signal. The following characteristics of the coherent spike have been observed:

(1) It peaks at zero delay time and has a peak-to-base ratio of the order of 1.5/1 to 2.5/1 and a FWHM of the order of 2.5–4 psec. This width contrasts with the FWHM of the

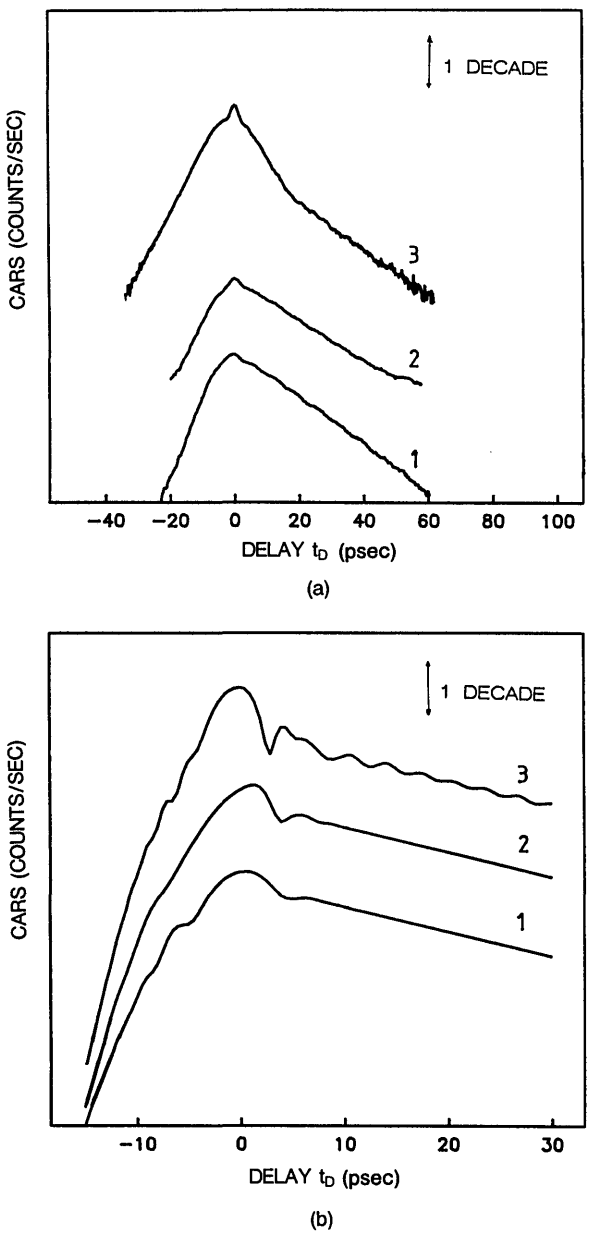

Fig. 3. (a) Experimental CARS time scans of the 656-cm^{-1} mode in liquid CS_2, showing the coherent spike under different conditions of excitation and/or probing. curve 1: $\delta_R = 1.2$ cm^{-1}, $\delta_D = 2.2$ cm^{-1}; curve 2: $\delta_R = -6.25$ cm^{-1}, $\delta_D = -7.3$ cm^{-1}; curve 3: $\delta_R = 5.0$ cm^{-1}, $\delta_D = 1.5$ cm^{-1}; the steep initial decay extends over 1.6 decades. (b) Simulated CARS signals, corresponding to the experimental conditions of (a): the experimental features are qualitatively reproduced. Within (a) and (b), all curves are plotted on the same vertical logarithmic scale, with arbitrary offset.

underlying broad structure, which is of the order of 10 (±2) psec. Typical examples are curves 2 and 3 of Fig. 3.

(2) It is not observed (or just barely observed) under on-resonance excitation conditions, $\delta_R \simeq 0$, as curves 1 of Fig. 3 illustrate. The residual enhancement on top of the curves is recognized as the so-called overshoot reported in Ref. 13.

If the Raman mode is excited off resonance, the following behavior of the material is expected. The electronic excitation always remains at the driving frequency, whereas the Raman oscillators relax from the same driving frequency to their resonant frequency ω_R. The CARS radiation due to the former excitation is at frequency $2\omega_L - \omega_S$, i.e., at the anti-Stokes frequency ω_{AS}, whereas that due to the latter excitation is at frequency $\omega_L + \omega_R$. Therefore essentially two situations of detection must be distinguished. Either the detection frequency is adjusted to the Raman oscillation: $\delta_D \simeq \delta_R$ (curves 2 in Fig. 3; the well-known exponential decay with characteristic time T_2 is observed, with a coherent spike sitting on top of it) or else (curves 3 of Fig. 3) the detection frequency is adjusted to the anti-Stokes frequency: $\delta_D \simeq 0$. For this last case, the coherent spike is still detectable, but the signal's strength has strongly decreased. The usual exponential decay sets in only in the tail of the signal, whereas for short delay times a steep quasi-instantaneous decay is observed.

(3) The spike shifts on top of the signal with a variation of the delay τ within the pump pair. Apparently, the spike is always centered at that value of t_D for which the yellow pump and probe beams coincide in time. This is demonstrated in the CARS runs of Fig. 4, each of which was recorded with a different value of τ. The coherent spike is centered at $t_D \simeq \tau$, whereas the top of the broad structure remains near zero delay.

(4) Switching to the configuration in which pump and probe beams have a mutually orthogonal polarization causes the spike to disappear, as exemplified in Fig. 5. Moreover, the signal now has a broad top, of ~ 4-psec width. According to the corresponding simulations, this originates in the delay of the *C* Raman contribution with respect to the other (*B*) contribution and to the instantaneous electronic one.

(5) If the mistuning of the laser frequencies δ_R is such that the driving frequency comes closer to the frequencies of nearby Raman modes from isotopes or hot bands, the oscillation of these sidebands gets stronger in comparison with that of the fundamental Raman mode. As a result, beats in the decaying tail of the CARS signal become observable. Such experiments might suggest that the central spike under discussion is just part of the beats. However, the comparison with the orthogonal polarization configuration proves that it is really a coherent spike, unrelated to the simultaneous excitation of several sidebands: the beats are still observable, but the spike has disappeared. Besides, as is illustrated in Fig. 3, the spike is equally well observed if no sidebands are excited at all (i.e., in CS_2: $\delta_R < 0$).

It turned out that only two sidebands of the fundamental 656-cm^{-1} mode are important for simulating the above experiments, namely, the hot band at 647.6 cm^{-1} and the ^{34}S isotope mode at 645.5 cm^{-1}.[22] The dominant beat reflected in the experimental signal corresponds to the 10-cm^{-1} beat between the 656- and 645.5-cm^{-1} modes.

(6) If an additional étalon is inserted into at least one of the dye lasers, while approximately the same values of mistuning and detection frequency are kept, the spike disappears. As was mentioned above (Sections 2 and 4), the insertion of an étalon improves the coherence of the dye laser, which in our model finds expression in a smaller chirp value. It is noteworthy that the time resolution is not essentially altered, although the insertion of an étalon broadens the pulse envelope by a factor of ~1.5.

The more general validity of the above results has been

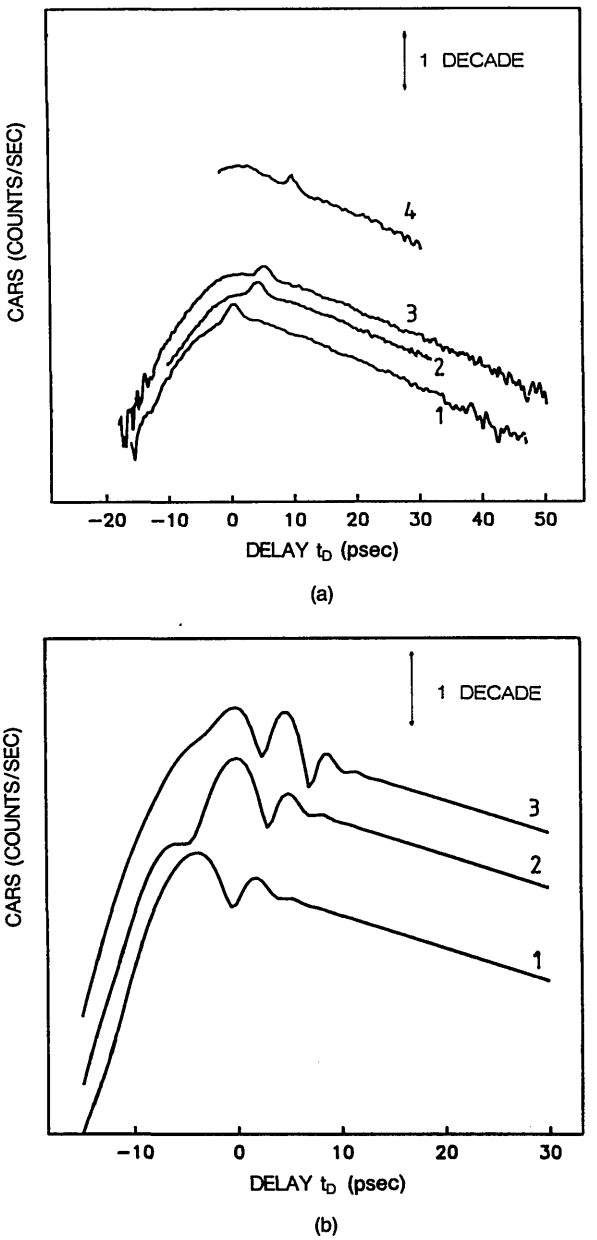

Fig. 4. Shift of the coherent spike with delay τ between both pump beams. (a) Experimental runs under the following conditions: $\delta_R = -12.2$ cm^{-1}, $\delta_D = -16.0$ cm^{-1}, and $\tau = 0$, 3.75, 5, and 10 psec in curves 1, 2, 3, and 4, respectively. $t_D = \tau$ corresponds to coincidence in time between both ω_L beams. (b) Simulated data: δ_R and δ_D are equal to the experimental values, τ varies from −5, over 0, to 5 psec in going from curve 1 to curve 3. The separate contributions to the total signal all exhibit approximately the same shift, of order τ. Within (a) and (b), all curves are plotted on the same vertical logarithmic scale, with arbitrary offset.

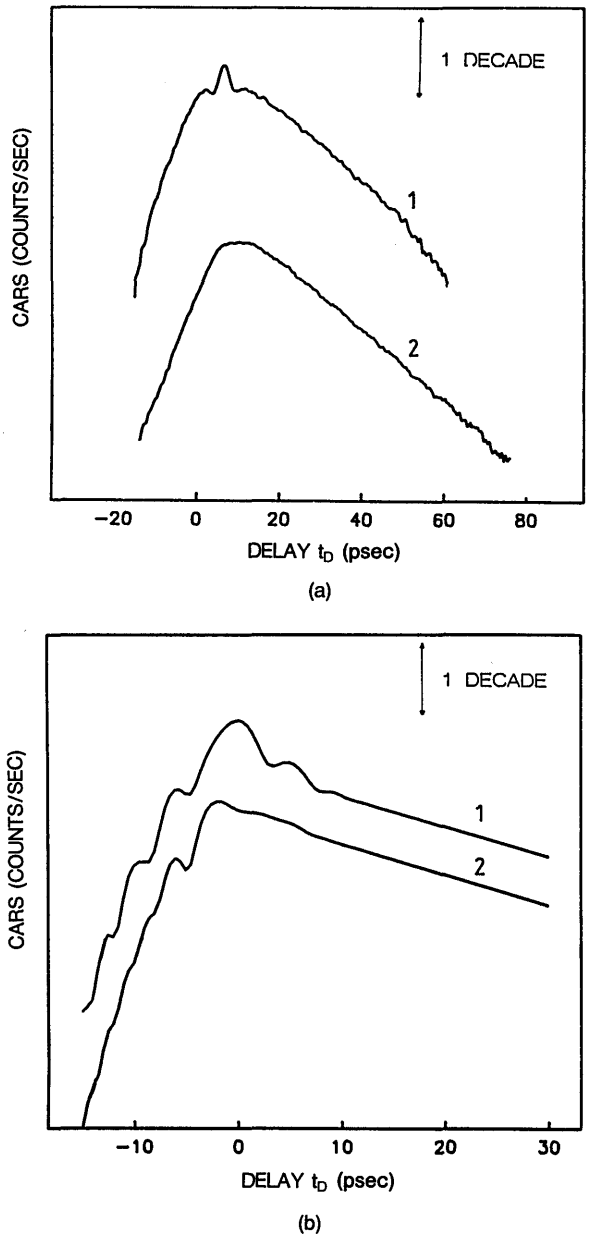

Fig. 5. Disappearance of the coherent spike in the orthogonal-polarization configuration. (a) Experimental CARS scans of the 656-cm^{-1} mode in liquid CS_2 with $\delta_R = -4.2$ cm^{-1} and $\delta_D = 0$ cm^{-1}. The polarizations of pump and probe beams were mutually parallel for curve 1 and orthogonal for curve 2. (b) Corresponding simulated data with the same values of δ_R and δ_D as in (a). The orthogonal polarization configuration (curve 2) is simulated by eliminating the *B* Raman contribution. Within (a) and (b), all curves are plotted on the same vertical logarithmic scale, with arbitrary offset.

confirmed by similar experiments and corresponding simulations on the breathing mode in liquid C_6H_6.

Our observations strongly indicate that the phase structure of the dye-laser pulses is responsible for the appearance of the coherent spike. The experiments with orthogonal polarization conditions, in which the *B* Raman contribution is almost eliminated, point out that the spike originates mainly in the interference between both Raman contributions. These conclusions are reinforced by the extensive numerical study that we have performed, of which the most important results have been presented in Figs. 3–7.

Only in the up–down configuration for the dye-laser chirps did the simulations reproduce the essential features of the experiments, in agreement with the conclusions drawn in Subsection 4.A.1 from the observed time resolutions. Particular evidence for our conclusions about the spike's origin comes from a comparison of simulations, run with different relative strengths of the electronic contribution, in Fig. 6. If the curves are counted from top to bottom, the electronic contribution is completely excluded in curve 2, whereas in curve 3 the electronic contribution is included but the *B* Raman contribution is excluded. Apart from the small bump around the top of the main *C* Raman contribution, all separate contributions have a smooth structure near zero delay. Therefore it is clear that the central coherent spike that appears in the normal situation (curve 1) in which all contributions are correctly accounted for arises almost completely from the interference between both Raman contributions.

Still, quantitative disagreements between experimental and simulated data as regards the relative magnitude of the spike and surrounding dips are observed. For instance, in curves 2 of Fig. 3 the experimental ratio is ~1.5/1, whereas in the corresponding simulation it is ~4.7/1. This difference can probably be explained by the uncertainty about the experimental pulse parameters for which the discrepancy between the observed cross-correlation width and the separate pulse widths derived from the respective autocorrelation traces gives an indication. At least part of the disagreement may be attributed to time jitter between the two dye lasers. We confirmed that as the relative jitter that is ascribed to the dye-laser pulses in the simulations increases, the discrepancy diminishes. If the disagreement between the simulated and experimental data resides in a fast oscilla-

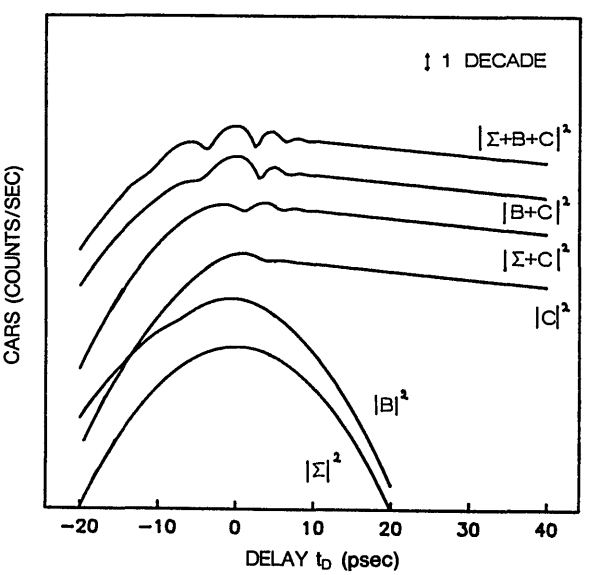

Fig. 6. Origin of the coherent spike, from a comparison between simulations that alternately exclude one of the separate contributions to the total observed CARS signal, as indicated by the curves. The squared separate contributions to the total CARS signal are also shown. Conditions are $\delta_R = \delta_D = -10$ cm^{-1}. All curves are plotted on the same vertical logarithmic scale, with arbitrary offset.

tory structure, the adoption of a small jitter value (which bridges the period of oscillation) brings the data into mutual agreement. In most cases, however, the jitter value that is required to make the discrepancy disappear is unreasonably large in comparison with the near-perfect synchronism to be expected in a double synchronously pumped dye-laser system.[23] We come to the same conclusions, however, if we are estimating the jitter from experimental correlation data. Here the edge of the jitter distribution is evaluated as one half of the root of the difference between the measured and expected squared widths of the intensity cross correlation between both dye lasers; the expected cross-correlation width is evaluated under the assumption of Gaussian pulses. It is not clear to us why the jitter thus obtained is ~8 psec, which is also too large to be realistic. An analogous problem has been addressed in Ref. 10.

Figure 7 illustrates the systematic influence of jitter in simulations of CARS time runs. The spike/base ratio decreases from 8/1 to 5/1 as the jitter parameter increases from 0 to 5. It has been verified that the influence of jitter is observed mostly in the interference term. For example, in this case of oppositely chirped pulses, under the influence of jitter the time resolution gets worse by only a factor of ~1.1.

An additional result of our numerical study is the gradual disappearance of the coherent spike as the spectral bandpass for detection is widened; an experimental confirmation of this is found in Ref. 5.

In summary, there are three good reasons for the fact that the coherent spike, as observed by us, has not to our knowledge been reported yet. Usually, (1) the CARS signal is not spectrally resolved, (2) the orthogonal polarization configuration is adopted (because the parallel situation only obscures the signal, without adding information about the Raman excitation), and (3) CARS experiments are not performed with a cw mode-locked dye-laser system. Only in the research reported in Ref. 5 was a similar phenomenon

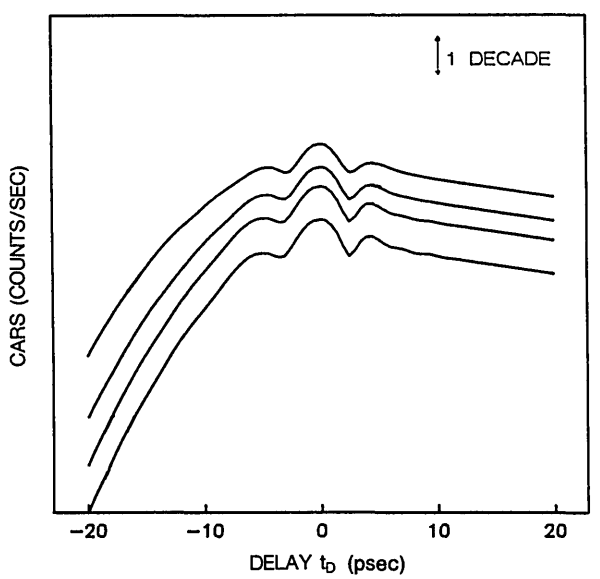

Fig. 7. Influence of jitter on the relative strength of the coherent spike. In going from the lowest to the upper simulated curve, the jitter parameter increases from 0, over 1.5 and 3, to 5 psec. Conditions are $\delta_R = \delta_D = -10$ cm^{-1}. All curves are plotted on the same vertical logarithmic scale, with arbitrary offset.

observed. The coherent spike's width and quasi-symmetrical shape near zero delay, and the role of the resonance conditions and of the detection spectral bandpass in its appearance, make it clearly distinguished from the overshoot of Ref. 13. We believe, however, that Holzapfel *et al.*[24] have observed the same phenomenon in CARS experiments with femtosecond synchronously pumped mode-locked dye lasers.

3. *Time and Spectral Characteristics with Different Chirps*

To substantiate the importance of the relative signs of the laser pulse chirps, we have performed some specific CARS and SRG experiments, of which the characteristics have a pronounced dependence on the chirps. We expect the chirp sign to be related to the position of the lasing frequency within the gain curve, as has been confirmed in Ref. 25. The dye laser should have upchirped (downchirped) pulses if tuned to the yellow (red) side of the gain curve maximum. Therefore the experiments discussed next are series of CARS or SRG measurements in which both dye lasers have been tuned across their gain curves simultaneously such that their frequency difference remains constant. The resulting signal characteristics should reveal the corresponding changes in the chirp signs:

(1) The first check consists of a series of spectrally resolved CARS measurements, in which the spectral position of the anti-Stokes peak due to the electronic contribution to the signal is monitored as a function of the probe delay t_D. It will be shown in Eq. (17) below that this peak position shifts proportionally to $(\beta_L + \beta_S)t_D$. The corresponding experiments, however, demonstrate that the precision and reproducibility required for convincing results cannot be attained with the present setup.

(2) According to simulations based on Ref. 2, the spectral width of the two-beam SRG signal R_{δ_R} as a function of excitation frequency has an inverse dependence on $|a_L\beta_L - a_S\beta_S|$. Hence it is expected to broaden in the upchirped–downchirped situation, in comparison with both the upchirped–upchirped and downchirped–downchirped situations. In the corresponding experiments, we checked the four-beam SRG time resolution R_t at the same time. The results of these experiments can be simulated with more than one choice of relative chirp sign, depending on the adopted amount of time jitter between both dye lasers. This is because jitter has different degrees of importance in different chirp configurations: the spectral width broadens proportionally to the sum of the chirp parameters $(\beta_L + \beta_S)$, and the time resolution narrows with the sum of the chirps. As a consequence, the up–down configuration is rather insensitive to jitter, but the up–up and down–down configurations show drastically changed characteristics. Since we are uncertain about the amount of jitter in our experiments, as explained in Subsection 4.A.2, these experiments have proved ambiguous for the purpose of determining the chirp signs.

(3) Analogously, we have examined numerically whether the characteristics of a two-beam CARS experiment are indicative for the chirps. Three parameters can be varied: the delay between the L and S laser pulses, their frequency mistuning, and the difference between the detection fre-

quency and the anti-Stokes frequency $2\omega_L - \omega_S$; one of the parameters is varied while the other two are kept fixed. It turns out that, unlike for SRG in which the L and S pulses play a symmetric role, their influence on the behavior of the two-beam CARS signal is clearly distinct. However, because of the interference between the electronic and Raman contributions, the overall behavior is too complicated to be valuable for our purpose.

In conclusion, the experiments described in this subsection have not added unambiguous evidence for our conclusion about the relative chirp signs in our laser system. It would be interesting to perform independent experiments that yield a more accurate characterization of the pulse parameters and, in particular, an unambiguous determination of the chirp sign.[26]

B. Critical Frequency Mistuning

In the past[15] we discussed the observation of a pronounced dip in SRG decay curves at specific values of the mistuning between the excitation frequency and the resonance frequency of the Raman mode. The phenomenon results from an interference effect between the driving fields and the response of the excited oscillator mode.

Until now, the values of critical frequency mistuning, $\delta_{R,c}$, were obtained from purely numerical simulations, in agreement with experimental data. Moreover, it was argued that the same phenomenon cannot be observed in CARS. In the present analysis, the critical values can be determined analytically in SRG as well as in CARS: we discuss these results first. The experimental appearance of the critical dip in CARS is discussed at the end of this section.

For both SRG and CARS, the Raman contributions, as a function of delay t_D, are written as an exponential times the complex complementary error function w [see Eqs. (12) for CARS and Ref. 2 for SRG]. Therefore the Raman term in the signal becomes zero only for these sets of parameters for which the function w equals zero. For example, the following (complex) zero points are recognized[27]: $\pm 2.675 - i2.2$ and $\pm 2 - i1.35$. The zero point chosen defines two relationships between the critical parameters; the constants that they contain depend on the pulse parameters and the Raman mode's T_2. For clarity, these relationships are listed explicitly:

For SRG:

$$1/(2\sqrt{\mathcal{A}})\{-\delta_{R,c} + a_L a_S(\beta_L + \beta_S)(\tau + \tau')/[2(a_L + a_S)]\} = \pm 2 \quad (\text{or } \pm 2.675)$$

and

$$1/(2\sqrt{\mathcal{A}})\{-2\mathcal{A}t_D + 1/T_2 + a_L(\tau - \tau')/2 + a_L\beta_L(a_L\beta_L - a_S\beta_S)(\tau - \tau')/[2(a_L + a_S)]\} = -1.35 \quad (\text{or } -2.2), \quad (15)$$

with

$$\mathcal{A} = [(a_L + a_S)^2 + (a_L\beta_L - a_S\beta_S)^2]/[4(a_L + a_S)]$$

and τ and τ' representing an eventual delay within the pump and probe pair, respectively.

For CARS:

$$\mathrm{Re}\{1/(2\sqrt{\alpha})[-\delta_{R,c} + \alpha\delta_D/A_L]\} - \mathrm{Im}\{1/(2\sqrt{\alpha})[-2\alpha t_D + 1/T_2 + 2A_L\alpha\tau/(A_L + A_S^*)]\} = \pm 2 \quad (\text{or } \pm 2.675)$$

and

$$\mathrm{Im}\{1/(2\sqrt{\alpha})[-\delta_{R,c} + \alpha\delta_D/A_L]\} + \mathrm{Re}\{1/(2\sqrt{\alpha})[-2\alpha t_D + 1/T_2 + 2A_L\alpha\tau/(A_L + A_S^*)]\} = -1.35 \quad (\text{or } -2.2). \quad (16)$$

An analysis of these relationships for SRG and CARS leads to the following conclusions:

(1) Concerning SRG, in agreement with Ref. 15 the value of the critical mistuning $\delta_{R,c}$ is independent of the time T_2 of the Raman mode. But here we prove that the delay value t_D at which the dip is observed does depend on T_2. In a normal SRG experiment, in which exact synchronism exists within the pump pair and the probe pair, $\tau = \tau' = 0$, the dip is observed for both $+\delta_{R,c}$ and $-\delta_{R,c}$ at the same delay time if the influence of the contributions other than the Raman one are negligible.

(2) For comparison with Ref. 15, the present pulse parameters have been reduced to the single correlation parameter γ_C that was used there for characterizing the correlation function that determines the Raman contribution in SRG experiments. We reproduce the same values 1.06 and 2.16 for the product $\gamma_C\delta_{R,c}/(2\pi)$ but find the additional value of 1.42 between.

(3) The relationships given for CARS in Eqs. (16) make only the C Raman contribution go to 0. In order to obtain the relationships corresponding to the B contribution, nothing but an exchange of τ with t_D is required. The resulting critical values are different for B and C.

(4) In CARS, in general, all parameters are mutually related in both relationships. Only in the limit of zero chirps does one retrieve a situation analogous to the one in SRG, except for the interplay between δ_R and δ_D. At any rate, the critical dip appears under different conditions, as compared with the situation for SRG.

(5) If the Eqs. (15) and (16) are reduced to the corresponding two-beam situations, it is remarkable that critical mistuning still appears in CARS for specific sets (δ_R, δ_D, $\tau \neq 0$) but not in SRG.

(6) In our CARS experiments, critical mistuning was not observed even if interferences were minimized by probing with an orthogonally polarized probe beam. This is because the previous discussion holds in the limit of infinitely small detection bandwidth centered at the critical detection frequency, whereas in our experiments the minimum allowed bandpass was ~ 1 cm^{-1}. Our simulations point out that integration of the detected signal over such a bandwidth washes out the critical dip. As an example of a CARS time run (Fig. 8), the critical dip should be detected at $t_D = 14$ psec, but it disappears as the detection bandwidth increases. For clarity, interferences with the B Raman contribution are excluded from these simulations.

These conclusions hold equally well with respect to spectral CARS scans: a zero C Raman contribution is observed

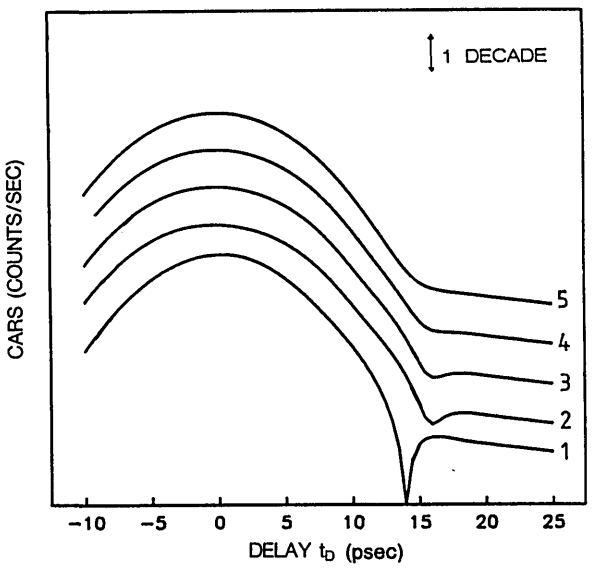

Fig. 8. Appearance of the critical frequency dip in CARS time run simulations. The critical conditions are $\delta_R = -7.94$ cm^{-1} and $\delta_D = -5$ cm^{-1}; correspondingly, the separate $|C|^2$ Raman contribution is zero at the critical delay value of 14 psec (curve 1). Curves 2–5 are simulations of the total CARS signal, in the orthogonal polarization configuration, for increasing values of the detection bandpass Δ: in going from 2 to 3 to 4 to 5, Δ assumes the values 0, 1, 2, and 4 cm^{-1}, respectively. All curves are plotted on the same vertical logarithmic scale, with arbitrary offset.

at the critical point but only in the limit of infinite spectral resolution.

As a consequence, in all CARS experiments that integrate the total anti-Stokes signal, corresponding to the situation discussed in Ref. 15, the phenomenon of critical mistuning cannot be observed.

C. CARS Spectra

Together with the time runs, the CARS signal has been studied as function of the detection frequency (spectrometer setting) at a fixed delay. These experiments are understood if the initial expressions of Eqs. (12) are interpreted as functions of δ_D at a fixed value of t_D and δ_R (with $\tau = 0$). The alternative experiment, in which the difference between the laser frequencies is tuned, is complicated by the presence of the Pellin–Broca prisms in the experimental setup (Fig. 1). Therefore we have not performed such experiments, but the results to be expected are derived below from our theoretical and numerical analysis by fixing δ_D and t_D (with $\tau = 0$) and varying δ_R:

(1) In the case of off-resonance excitation, $\delta_R \neq 0$, the observed spectrum in δ_D spans the region between δ_R and 0. As the delay increases, it may split into two separate peaks, centered at $\delta_D = \delta_R$ and at $\delta_D = 0$. According to the physical interpretation given in point (2) of Subsection 4.A.2, the former peak is attributable solely to Raman contributions and the latter to electronic excitations in particular. For still larger delays, the electronic peak disappears, since it decays with the pulse-correlation function. The relative strengths and intrinsic widths of the two peaks, and the corresponding relevant values of delay, depend on several parameters, among which are the value of δ_R, the pulse durations, and T_2. These features are confirmed by simulations, for instance in Fig. 9. Here typical experimental parameters have been selected, but chirps have been excluded in order to reveal the fundamental characteristics.

(2) In some experiments the center position of the spectral peak of electronic origin is seen to shift with t_D.

Quantitatively the above experimental data turned out to be highly sensitive to the exact experimental circumstances, but qualitatively the basic features are always observed to some extent. As is discussed explicitly below, the presence of chirp causes time-dependent shifts of the different contributions to the signal that have nothing to do with the relaxation of the Raman oscillators. This explains why experimentally the fundamental material response is less clearly distinguishable.

The characteristics of CARS spectra are traced in the theoretical formulas [Eqs. (12)] for the separate electronic and C Raman contributions as follows. First, we concentrate on the exponential factor, $|\exp(-\gamma)|^2$, that governs both the electronic and Raman contributions. For the present purpose, it is rewritten as

$$|\exp(-\gamma)|^2 = \exp\{-[\delta_D - t_D a_L a_S(\beta_L + \beta_S)/(2\,\mathrm{Re}\,A)]^2 \times \mathrm{Re}\,A/(2|A|^2)\}\exp[-a_L(a_L + a_S)t_D{}^2/(2\,\mathrm{Re}\,A)]. \quad (17)$$

This equation tells us that the shift of the electronic peak is proportional to the sum of the dye-laser chirps. The analogous phenomenon, translated into CARS time runs, results in a delay of the electronic signal maximum with the detec-

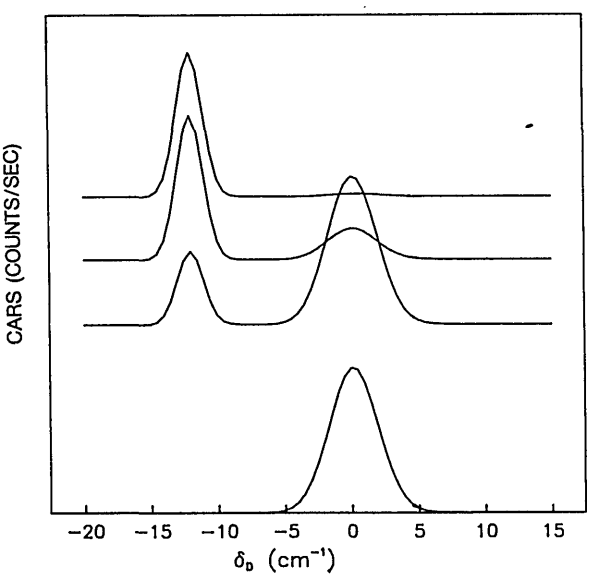

Fig. 9. CARS spectra at delay times t_D of 21, 24, 25, and 26 psec, respectively (from lower to upper curves), simulated on the assumption of transform-limited Gaussian pulses of duration $t_{p,L} = 6.36$ psec and $t_{p,S} = 5.25$ psec, with $\delta_R = -12$ cm^{-1}. The peak shift to $\delta_D = \delta_R$ is due to the C Raman contribution; the B and Σ contributions remain centered at $\delta_D = 0$ cm^{-1}. The vertical scale is linear; each curve is normalized to its own maximum. Notice that the peak width (FWHM) of the total signal, at $t_D = 26$ psec, is determined essentially by the C Raman contribution and is 2.3 cm^{-1}, whereas the peak width of the total signal at $t_D = 0$ psec is 4.3 cm^{-1}. With regard to shape, the spectra remain identical for $t_D > 26$ psec.

tion frequency that is again proportional to this sum of chirps. The small shifts that have been observed experimentally, in contrast with the large absolute values of chirp of each dye-laser pulse separately, are due to operation of our setup with opposite chirp signs.

The electronic FWHM(δ_D) to be expected is

$$\mathrm{FWHM}(\delta_D) = 2\{[\ln 2(2a_L + a_S)][1 + (2a_L\beta_L - a_S\beta_S)^2/(2a_L + a_S)^2]\}^{1/2} \quad (18)$$

or else, in the absence of chirps,

$$= (2\Delta\omega_L{}^2 + \Delta\omega_S{}^2)^{1/2}, \quad (19)$$

with $\Delta\omega_{L(S)}$ being the $L(S)$ laser spectral width. Under the influence of chirp, it generally broadens, as expected from the corresponding broadening of the laser spectral widths.

Second, the quantitative behavior of the C Raman contribution is estimated from the combined effects of the above exponential factor and the complex error function. The parameter mistuning enters into the latter factor. In order to simplify the following discussions, chirps are temporarily excluded; their influence can be retrieved from the full expressions given in Eqs. (12) and the corresponding numerical simulations.

The shift of the Raman peak results from the competition between the exponential and the complex error function w. The former causes the same shift as for the electronic contribution, whereas the latter, at any value of t_D, is largest if the real part of its argument is zero (except in the neighborhood of the critical point). This condition makes the Raman peak shift toward δ_R. This tendency gets dominant at large enough values of t_D, i.e., for

$$T_2 t_D \gg 1/(2\alpha),$$

with

$$1/(2\alpha) = \frac{1 + 2t_{p,S}{}^2/t_{p,L}{}^2}{1 + t_{p,S}{}^2/t_{p,L}{}^2}[t_{p,L}{}^2/(4\ln 2)]. \quad (20)$$

This condition on $t_D T_2$ is dependent almost entirely on the L-laser pulse width, for the right-hand-side of the inequality varies only from $t_{p,L}{}^2/(4\ln 2)$ to $2t_{p,L}{}^2/(4\ln 2)$ in going from the limit $t_{p,L} \gg t_{p,S}$ to the limit $t_{p,L} \ll t_{p,S}$. Note the inverse proportionality between t_D and T_2 for fixed laser pulse parameters.

As long as $t_D \ll 1/(2\alpha T_2)$, the spectral width of the Raman peak is independent of t_D and equal to that of the electronic peak. It narrows as the delay better satisfies condition (20). In the limit of infinitely large delay ($t_D \to +\infty$), the behavior of the Raman contribution is determined by

$$\exp\{1/(2\alpha T_2{}^2)\}\exp\{-2t_D/T_2\} \times \exp\{-(\delta_D - \delta_R)^2/(2A_L) - \delta_R{}^2/[2(A_L + A_S)]\}. \quad (21)$$

Therefore, finally, the Raman peak is a Gaussian, centered at $\delta_D = \delta_R$, and has a FWHM equal to $\Delta\omega_L$, independently of $\Delta\omega_S$. Its strength decreases exponentially with $2t_D/T_2$. As such, we have obtained the short-excitation, prolonged-interrogation results[16] from a strict analysis, and in addition we have proved that these results hold independently of the relative ratios of the L and S pulse widths. The only restriction on the choice of pulse widths resides in the overall signal attenuation factors.

The behavior of the Raman contribution as a function of the mistuning frequency δ_R can be discussed in a similar way. In order to determine the Raman characteristics in the limit of infinite delay, the last exponential factor in relation (21) is rewritten as

$$\exp\{-[\delta_R - \delta_D(A_L + A_S)/A]^2/(2\alpha) - \delta_D{}^2/(2A)\}; \quad (22)$$

it elucidates the Raman characteristics in the assumption of infinitely small detection bandpass. In this kind of experiment, however, one mostly samples the CARS signal integrated over its full bandwidth. Integration of Eq. (22) over δ_D yields

$$\sqrt{2\pi A_L}\exp\{-\delta_R{}^2/[2(A_L + A_S)]\}. \quad (23)$$

Therefore, as a function of laser mistuning, the Raman contribution has become a Gaussian, centered at zero mistuning; its FWHM is equal to $(\Delta\omega_L{}^2 + \Delta\omega_S{}^2)^{1/2}$, again independently of the ratio of the separate pulse widths. These characteristics should be compared with the simulated results at $t_D = 0$: the shape is between Lorentzian and Gaussian, the center position may slightly deviate from 0, and the width is also dependent on $1/T_2$.

In the literature, until now analytical estimates of the line-narrowing effects referred only to the limiting situations of short excitation and prolonged interrogation or prolonged excitation and short interrogation, always at probe delay times tending to infinity.[16] The advantage of our analysis is twofold: The evolution of linewidth with increasing delay t_D can be studied and the pulse parameters, including the influence of chirp, can be varied. Yet it is not possible to simulate three different laser pulses for excitation and probing, which inhibits direct comparison with the prolonged-excitation–short-interrogation results, but such extension of our analysis is straightforward.

5. CONCLUSIONS

This study has shown that picosecond dephasing experiments are as feasible with the same mode-locked dye-laser system with the CARS as with the SRG technique.

As regards experimental convenience, the requirement of an elaborate high-frequency modulation-detection technique[2,3,28] in SRG must be weighed against the need for a spectrometer plus photon-counting equipment and careful background suppression in spectrally resolved CARS. SRG has several advantages: It is quasi-insensitive to phase-matching requirements. For instance, the CARS technique is proved unfit for time-resolved experiments in a diamond anvil cell for high-pressure studies because the aperture angle required in phase-matched conditions is not accessible. SRG provides a better time resolution owing to its higher sensitivity to the coherence properties of the applied laser pulses. Essentially, this stems from the fact that SRG is governed by a four-field correlation function and CARS by the intensity correlation of three fields. The dynamic ranges achieved in both techniques are quasi equivalent: ~4.5 decades in CARS and more than 2 decades in SRG, when both are performed on the same system, namely, the 656-cm^{-1} mode in liquid CS_2 at room temperature.

This study has also concentrated on the appearance of a

coherent spike in time-resolved CARS, centered at zero delay. The spike originates in the interference of two Raman contributions in the total signal (which are indistinguishable at zero delay). It shows up in our simulations in quite good agreement with the experimental data, if we take into account that our laser pulses are linearly chirped Gaussians of opposite chirp sign and that the detection is spectrally selective. Some discrepancies still exist between the experimental and simulated data: we believe that they originate in the fact that our pulse model is not fully adequate for describing the mode-locked pulses of our dye lasers. Probably a stochastic factor must be included, in the pulse amplitude as well as in its phase. More-precise experiments are needed for characterizing the pulses more accurately.

ACKNOWLEDGMENTS

We are indebted to R. Sprik for interesting discussions and to E. Spaans for his collaboration in the experiments. The research of M. De Mazière has been made possible by a fellowship from the Royal Dutch Academy of Arts and Sciences. We gratefully acknowledge financial support from the Stichting voor Fundamenteel Onderzoek der Materie, which is part of the Nederlandse Organisatie voor Wetenschappelijk Onderzoek.

A. Lagendijk is also with the Institute for Atomic and Molecular Physics, Stichting voor Fundamenteel Onderzoek der Materie, Kruislaan 407, 1098 SJ Amsterdam, The Netherlands.

* Present address, Belgian Institute for Space Aeronomy, Ringlaan 3, B-1180 Brussels, Belgium.

† Present address, IBM T. J. Watson Research Center, P.O. Box 218, Yorktown Heights, New York 10598.

REFERENCES AND NOTES

1. A. Laubereau and W. Kaiser, Rev. Mod. Phys. **50,** 607 (1978); A. Penzkofer, A. Laubereau, and W. Kaiser, Prog. Quantum Electron. **5,** 55 (1979).
2. M. De Mazière, Ph.D. dissertation (University of Antwerp, Antwerp, 1986); M. De Mazière, C. Sierens, and D. Schoemaker, "Analysis of dephasing signal in picosecond stimulated Raman gain experiments," J. Opt. Soc. Am. B (to be published).
3. M. Van Exter and A. Lagendijk, Opt. Commun. **56,** 191 (1985); M. Van Exter, Ph.D. dissertation (University of Amsterdam, Amsterdam, 1988).
4. C. H. Lee and D. Ricard, Appl. Phys. Lett. **32,** 168 (1978).
5. F. M. Kamga, Ph.D. dissertation (University of Rochester, Rochester, N.Y., 1980); F. M. Kamga and M. G. Sceats, Opt. Lett. **5,** 126 (1980).
6. B. H. Hesp and D. A. Wiersma, Chem. Phys. Lett. **75,** 423 (1980); K. Duppen, B. M. M. Hesp, and D. A. Wiersma, Chem. Phys. Lett. **79,** 399 (1981).
7. B. K. Rhee, W. E. Bron, and J. Kuhl, Phys. Rev. B **30,** 7358 (1984); J. Kuhl and D. von der Linde, in *Picosecond Phenomena III,* K. B. Eisenthal, R. M. Hochstrasser, W. Kaiser, and A. Laubereau, eds. (Springer-Verlag, Berlin, 1982), p. 201.
8. F. Ho, W.-S. Tsay, J. Trout, S. Velsko and R. M. Hochstrasser, Chem. Phys. Lett. **97,** 141 (1983); S. Velsko, J. Trout, and R. M. Hochstrasser, J. Chem. Phys. **79,** 2114 (1983); S. Velsko and R. M. Hochstrasser, J. Phys. Chem. **89,** 2240 (1985).
9. M. C. Nuss, W. Zinth, and W. Kaiser, J. Opt. Soc. Am. B **2,** 322 (1985).
10. L. Angeloni, R. Righini, E. Castelucci, P. Foggi, and S. Califano, J. Phys. Chem. **92,** 983 (1988).
11. D. D. Dlott, C. L. Schosser, and E. L. Chronister, Chem. Phys. Lett. **90,** 386 (1982); T. J. Kosic, R. E. Cline, Jr., and D. D. Dlott, Chem. Phys. Lett. **103,** 109 (1983).
12. N. Kohles and A. Laubereau, Appl. Phys. B **39,** 141 (1986); Chem. Phys. Lett. **138,** 365 (1987).
13. N. Kohles, P. Aechtner, and A. Laubereau, Opt. Commun. **65,** 391 (1988).
14. W. Zinth and W. Kaiser, Opt. Commun. **32,** 507 (1980); W. Zinth, H.-J. Polland, A. Laubereau, and W. Kaiser, Appl. Phys. B **26,** 77 (1981); A. Laubereau, H. R. Telle, and G. M. Gale, Appl. Phys. B **34,** 23 (1984).
15. M. Van Exter, A. Lagendijk, and E. Spaans, Opt. Commun. **59,** 411 (1986).
16. W. Zinth, M. C. Nuss, and W. Kaiser, Chem. Phys. Lett. **88,** 257 (1982); Opt. Commun. **44,** 262 (1983); M. C. Nuss, W. Zinth, and W. Kaiser, J. Opt. Soc. Am. B **2,** 322 (1985); M. A. Collins, P. A. Madden, and A. D. Buckingham, Chem. Phys. **94,** 291 (1985).
17. E. Hecht and A. Zajac, *Optics* (Addison-Wesley, Reading, Mass., 1974), p. 131.
18. We have defined a measure for the deviation from transform-limitedness as the difference between the actual time–bandwidth product and the transform-limited value, relative to the latter.
19. R. W. Hellwarth, Prog. Quantum Electron. **5,** 1 (1977).
20. If the anisotropic part of the Raman response function is taken into account in Eq. (4), then in the parallel-polarization configuration the response function becomes

$$d_R(t) = -ia^2[1 + 4/45b^2/a^2 \exp(-t/T_{\rm rot})]\exp(-t/T_2) \times \exp(-i\omega_R t)\Theta(t) + \text{c.c.} \quad (24)$$

for both Raman contributions, whereas in the orthogonal polarization configuration it becomes

$$-ib^2/15 \exp(-t/T_{\rm rot})\exp(-t/T_2)\exp(-i\omega_R t)\Theta(t) + \text{c.c.} \quad (25)$$

for the B Raman contribution and

$$-ia^2[1 - 2/45b^2/a^2 \exp(-t/T_{\rm rot})]\exp(-t/T_2)\exp(-i\omega_R t)\Theta(t) + \text{c.c.} \quad (26)$$

for the C Raman contribution. Here a and b are proportional to the isotropic and anisotropic parts of the Raman polarizability tensor, respectively, and $T_{\rm rot}$ denotes the reorientational relaxation time in the liquid. See also B. Dick, Chem. Phys. **113,** 131 (1987).
21. For the 656-cm^{-1} mode in liquid CS_2, the depolarization ratio is ~13%, implying a b^2/a^2 ratio of ~2.36, and the reorientational time is ~2.1 psec. These parameters are taken from S. Ikawa and E. Walley, J. Chem. Phys. **85,** 2538 (1986); **86,** 1836 (1987); E. Spaans, M. Van Exter, and A. Lagendijk, "Measurements of rotational diffusion with time-resolved stimulated anisotropic Raman scattering," submitted to Opt. Commun.
22. Their parameters of relevance were taken from G. M. Gale, P. Ranson, and M. Denariez-Roberge, Appl. Phys. B **44,** 221 (1987). They are, for the 647- (645.5-) cm^{-1} mode, 30% (8%) integrated intensity relative to the fundamental mode and 5- (21-psec) relaxation time. The relaxation time of 5 psec is determined only as an upper limit; however, we have checked that the overall result is quite independent of its exact value.
23. D. von der Linde, Appl. Phys. B **39,** 201 (1986).
24. W. Holzapfel, R. Leonhardt, and W. Zinth, Appl. Phys. B **47,** 307 (1988).
25. U. Stamm, Appl. Phys. B **45,** 101 (1988); S. de Silvestri, P. Laporta, and O. Svelto, IEEE J. Quantum Electron. **QE-20,** 533 (1984).
26. To this end, we did pulse compression experiments with a grating pair: they yielded ambiguous results. Any other pulse characterization techniques available to us at present yield information only on the chirp's absolute value.
27. M. Abramowitz, I. A. Stegun, *Handbook of Mathematical Functions* (Dover, New York, 1972).
28. M. De Mazière and D. Schoemaker, J. Appl. Phys. **58,** 1439 (1985); M. Van Exter and A. Lagendijk, Rev. Sci. Instrum. **57,** 390 (1986).